# Molecular insight into the simultaneous capture of sarin/soman by graphene incorporating dual metal sites

Julien Claudot, Estelle Soubeyrand-Lenoir, Guillaume Maurin

# Molecular insight into the simultaneous capture of sarin/soman by graphene incorporating dual metal sites

Julien Claudot [a,b], Estelle Soubeyrand-Lenoir[b], Guillaume Maurin[a*]

[a] ICGM, Univ. Montpellier, CNRS, ENSCM, Montpellier, France

[b] DGA Maître NRBC, BP N°3-5 rue Lavoisier, 91710 Vert le Petit, France.

**Abstract**

Competitive adsorption of two major Chemical Warfare agents (CWAs), soman and sarin, was explored on a multi-site embedded graphene model integrating transition metal atoms (Cr, V and Zn). *Ab-initio* Molecular Dynamics simulations were performed to determine the most probable configurations of these CWAs on the graphene substrate. Further Density Functional Theory geometry optimizations revealed that both soman and sarin adopt a single-adduct configuration on a metal site whatever the nature of metal pairs considered, a scenario similar to that encountered for graphene embedding only 1 metal site. This result strongly suggests that each metal site present in real activated carbons is effective for the capture of these CWAs. To understand the effect of humidity, which is a major shortcoming in the field of air protector devices, further calculations were carried out in the presence of water molecules. We demonstrated that water does not dramatically impact the strength of interactions between these CWAs and both Cr and V metals while there is a substantial drop in the case of Zn metals. This trend was explained in light of further electronic analysis. This conclusion suggests that the use of Cr or V metal enables to maintain an efficient capture of CWAs under humidity while for Zn it is far to be the case.

## 1. Introduction

Capturing chemical warfare agents (CWAs), especially nerve agents such as sarin and soman is a major concern in modern warfare [1]. Despite the international ban on their uses [2], a few countries and terrorist organizations still possess stockpiles of these chemical weapons for potential sporadic attacks [3-6]. Personal air purifying respirator cartridges containing efficient adsorbent porous materials appear as a reliable solution to protect civilian or military individuals against these hazardous CWAs [7, 8]. Large surface area, high chemical stability and possible impregnation with transition metal atoms [9-13] have positioned activated carbons (AC) materials [14-18] as the current best adsorbents to capture a wide range of CWAs. In this field, most of the theoretical studies on adsorption of CWAs and related molecules by AC materials have been performed from a macroscopic standpoint to assess the lifetime of commercial cartridges [19, 20] under different conditions [21-23]. In contrast, few molecular simulation investigations [24-28] have been reported so far on the adsorption mechanism and they focused exclusively on small organic molecules such as hydrogen cyanide (HCN), benzene ($C_6H_6$) carbon monoxide (CO) [27, 29-31] or CWAs simulants, e.g. dimethyl methylphosphonate (DMMP) [32, 33]. To address this lack of fundamental understanding, we have initiated recently a computational study at the density functional theory (DFT) level with the aim to reveal the microscopic origin of the capture of CWAs by carbons impregnated with a series of metal sites [34, 35]. In these previous works, a graphene layer embedding a single transition metal atom was considered as a first model system to represent the AC adsorbents integrated into protection masks. These calculations systematically explored the interactions between a single sarin and soman molecule and a series of metal-impregnated carbon substrates in the presence/absence of water, in terms of adsorption sites and associated energetics. Typically, graphene substrates embedding either Chromium and Vanadium metal sites were demonstrated to ensure an efficient capture of sarin and soman in dry conditions [34], this attractive level of performance being maintained even under humidity [35]. As a further stage, herein we aim to gain insight into the competitive adsorption of CWAs on graphene substrates incorporating multiple metal sites, i.e. Cr, V and Zn. This scenario corresponds to a more realistic description of the currently used impregnated AC carbons for the capture of these target toxic molecules, which are known to incorporate different nature of metal sites [36, 37]. Further, in complement to our previous DFT studies [34, 35], here these whole systems were explored dynamically using *ab-initio* molecular dynamics (AIMD).

## 2. Computational details

Two carbon models were first built to model the adsorption of CWAs on a single metal and multi-metal embedded substrates. A $6 \times 6$ graphene sheet ($17.22\,\text{Å} \times 17.22\,\text{Å}$) with one carbon atom substituted by a transition metal atom (Chromium or Zinc) was considered to model a single site adsorption substrate (labeled as *metal@graphene)*. A $7 \times 7$ graphene sheet ($19.68\,\text{Å} \times 19.68\,\text{Å}$) was equally constructed with two carbon atoms substituted by transition metal atoms (Chromium, Vanadium or Zinc) to represent a multi-site substrate model (labeled as *metal1-metal2@graphene)* with a metal-metal distance arbitrary considered as ~10 Å. A length of 30 Å along the z-direction was considered for both models to avoid interactions between periodically replicated neighbors. One molecule of each CWA, i.e, sarin and soman was then incorporated on these two models using a different set of initial configurations. All AIMD simulations were carried using the program CP2K [38] with the Quickstep module [39] using dual basis set of Gaussian type orbitals (DZVP-molopt [40]) with plane-waves (with a cut-off $E_{cut} = 300\,Ry$). The PBE [41] functional, completed with DFT-D2 [42] corrections was considered to model the exchange-correlation energy and the dispersion correction. All AIMD simulations were performed at 300K for 8 ps, using a Nosé-Hoover thermostat and a 0.5 fs time step with $10^{-5}$ Hartree accuracy.

The impact of humidity on the competitive adsorption of sarin and soman on a single site metal embedded graphene was further considered with the introduction of 1 water molecule on the sarin/soman-*metal@graphene* configuration. In this case, AIMD simulations were followed by DFT geometry optimizations using Quantum Espresso package [43] at the DFT+D2 level in order to make a further energetics analysis. Ultrasoft Vanderbilt pseudopotentials [44] were used to describe ion cores of atom. An energy cut-off of 80 Ry was applied in combination with a convergence criteria on the energy of $1 \times 10^{-5}$ Ry. A Gaussian smearing with $\sigma = 0.01$ was employed for the two transition metals. Monkhorst-Pack grids of k-points replicating the graphene sheet dimensions was considered.

The adsorption energy of each individual CWA in the case of sarin/soman/H₂O/metal@graphene was defined as follows:

$$E_{ads}^{sarin} = E_{sarin/soman/H_2O/Metal@graphene} - (E_{sarin} + E_{soman/H_2O/Metal@graphene})$$

$$E_{ads}^{soman} = E_{sarin/soman/H_2O/Metal@graphene} - (E_{soman} + E_{sarin/H_2O/Metal@graphene})$$

Such a definition of the adsorption energy for each CWA allows the evaluation of the role of water on the strength of the CWA/substrate interactions in the presence of another CWA.

### 3. Sarin/Soman competitive adsorption on Cr@graphene and Zn@graphene

**Fig. 1 (a-b)** reports AIMD equilibrated configurations for the competitive adsorption of sarin and soman on both Cr@graphene and Zn@graphene. Single component adsorption energies, for sarin/Cr@graphene and soman/Cr@graphene, have been reported in our previous studies to be -43.84 kcal.mol$^{-1}$ and -39.71 kcal.mol$^{-1}$ respectively [34]. Indeed, on the same embedded chromium site, the adsorption of sarin is expected to be favored over soman. Starting with an initial configuration where both CWAs are 7 Å away from the metal site, our AIMD calculations confirmed that from a dynamics point of view the presence of a Cr site attracts more sarin over soman leading to a final states where the oxygen atom of sarin interacts preferentially with Cr atom in a similar way our previous static DFT calculations evidenced for the single component adsorption scenario [34]. This preferential adsorption mode of sarin pushes soman away from the Cr site as illustrated in **Fig. 1 (a)**. Our objective was then to verify if the same conclusion remains true even in the presence of metal site that shows only moderate affinity to sarin. Typically, Zn atom was considered since it was previously demonstrated by our DFT calculations to exhibit the weakest interactions with sarin from the full list of metals that were tested with an associated adsorption energy of -28.32 kcal.mol$^{-1}$ [34]. The resulting equilibrated AIMD configuration reported in **Fig. 1 (b)** is similar to that obtained in the case of the Cr site. This observation highlights that regardless to the magnitude of the sarin/metal interactions, sarin is expected to be preferentially adsorbed over soman once the two species are concomitantly present.
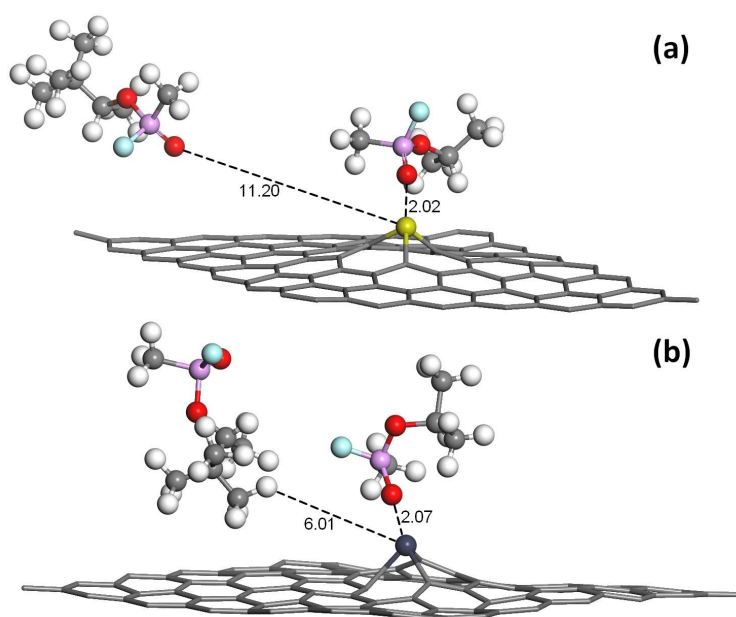
**Figure 1:** (a) Sarin/soman/Cr@graphene and (b) sarin/soman/Zn@graphene AIMD equilibrated structures. The reported distances are expressed in Å. C, O, F, P, H, Cr and Zn atoms are represented in grey, red, cyan, purple, white, yellow and dark blue respectively.

### 4. Sarin adsorption on a multi-metal embedded substrate Cr-V@graphene vs Cr-Zn@graphene

**Fig. 2 (a-b)** report the AIMD equilibrated structures for sarin adsorbed on multiple adsorption Cr-V sites. One observes that depending on the initial configurations, sarin is found to be adsorbed either on Cr or V sites with corresponding O(sarin)-Metal distances of 2.04 Å and 2.07 Å respectively that are reminiscent to those previously simulated for the single component adsorption [34]. The two configurations are characterized by very similar total energies (**Table S1**) and therefore they are almost equiprobable. This observation is in line with the equivalent single component adsorption energies previously reported for sarin on Cr@graphene and V@graphene, i.e., -43.84 kcal.mol$^{-1}$ and -43.00 kcal.mol$^{-1}$ respectively.
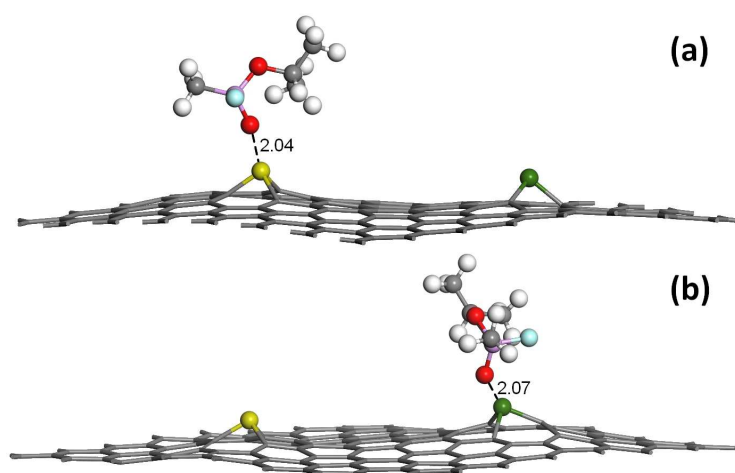


**Figure 2:** (a) Sarin/Cr-V@graphene and (b) sarin/V-Cr@graphene AIMD equilibrated structures. The reported distances are expressed in Å. C, O, F, P, H, V and Cr atoms are represented in grey, red, cyan, purple, white, green and yellow, respectively.

In contrast when the Cr/Zn pair is considered, **Fig. 3** shows that sarin is preferentially attracted by Cr consistent with a higher sarin adsorption energy for Cr vs Zn in the case of single metal site (-43.84 kcal.mol$^{-1}$ for Cr vs -28.32 kcal.mol$^{-1}$ on Zn [34]). All together, these simulations revealed that (i) the co-existence of Cr and V is expected to fix the first sarin molecules immediately since these two available metal sites equiprobably adsorb strongly sarin, while the presence of Zn in tandem with Cr is not expected to make a plus value for the adsorption of the first molecules since these molecules are preferentially adsorbed to Cr; and (ii) the presence of two neighbor

metal sites does not change the adsorption modes of sarin in both cases suggesting that that the impregnated carbon is expected to maintain a single-adduct adsorption of the CWA on the metal sites distributed in the impregnated carbons.
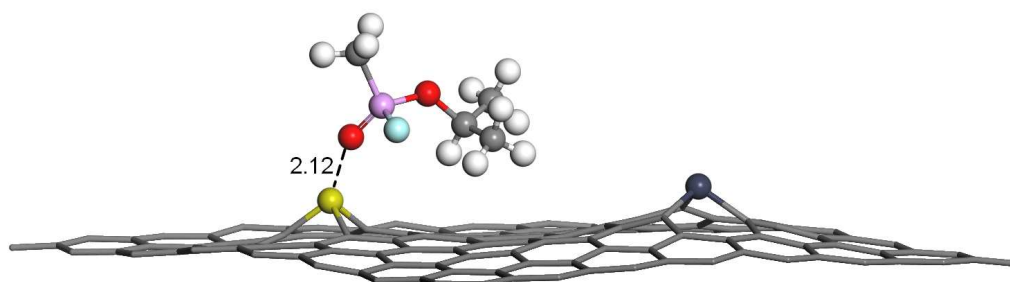


**Figure 3:** Sarin/Cr-Zn@graphene AIMD equilibrated structure. The reported distance is expressed in Å. C, O, F, P, H, Cr and Zn atoms are represented in grey, red, cyan, purple, white, yellow and dark blue respectively.

### 5.  Simultaneous adsorption on a multi-metal embedded substrate.

**Fig. 4 (a)** reports AIMD equilibrated structures for the competitive adsorption of sarin and soman on a dual Cr-Cr@graphene substrate. Starting with both molecules 7 Å away from each other and from the metal sites, one observes that both sarin and soman interact as single adducts over the two metal sites with characteristic O(CWA)-Cr distances similar to those obtained in the presence of a single metal site consistent with weak sarin/soman interactions and separating distances over 4 Å. The same conclusion can be drawn with the consideration of graphene substrates integrating V-V and Cr-V metal sites as illustrated in **Fig. S1 (a, b and c)**.
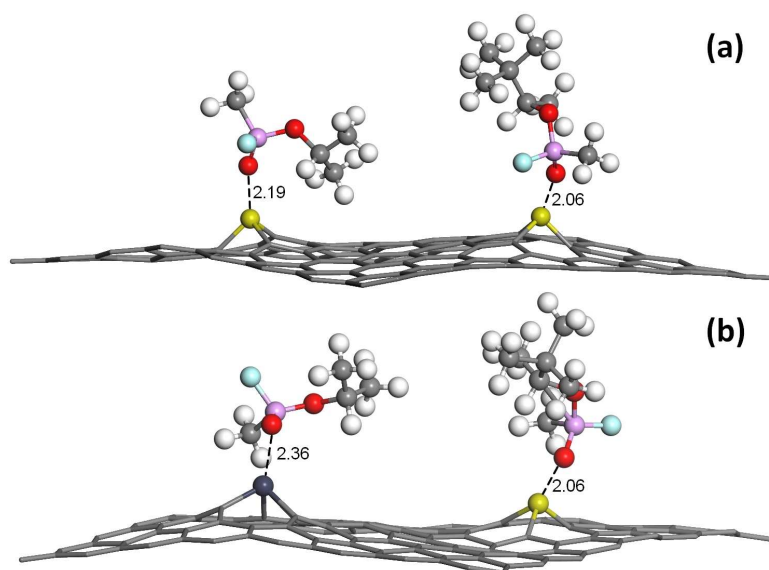
**Figure 4:** (a) Sarin/soman/Cr-Cr@graphene and (b) sarin/soman/Zn-Cr@graphene AIMD equilibrated structures. The reported distances are expressed in Å. C, O, F, P, H, Cr and Zn atoms are represented in grey, red, cyan, purple, white, yellow and dark blue respectively.

**Fig. 4 (b) and Fig. S2** further reports AIMD equilibrated structures of sarin and soman adsorption on Zn-Cr@graphene and Cr-Zn@graphene respectively. One still observes in all cases a single-site adduct towards the metal sites. The interacting sarin/Cr and soman/Cr distances of 2.14 Å (**Fig. S2**) and 2.06 (**Fig. 4 (b)**) Å respectively are as short as in the case of Cr-Cr@graphene (**Fig. 4 (a)**). This clearly confirms that the presence of Zn does not weaken the strength of interactions between the Cr sites and the CWAs. One notes for Zn that the interacting distances to both sarin (2.36 Å) and soman (2.77 Å) are significantly longer than the value obtained for a single Zn metal with sarin (2.01 Å) [34]. This emphasizes that the adsorption of the two CWAs on Zn is expected to be much weaker than on Cr.

To further illustrate the characteristics of Zn within these systems, Projected Density of States (PDOS) of orbitals of the substrate and CWAs atoms was carefully analyzed and reported on **Fig. 5**. PDOS is shown in such a way to present the contributions of p- orbitals of O and C atoms of CWAs, p- orbitals of C of the graphene sheet and the d- orbitals of transition metal atoms. Regarding the sarin/soman adsorbed on a dual Cr-Cr@graphene the resulting PDOS presented in **Fig. 5 (a)** shows two features, similarly as PDOS for a single Cr site embedded graphene reported in our previous study [34], i.e., (i) an important hybridization of d- orbitals of Cr with p-orbitals of carbon (graphene) at Fermi level, emphasizing the adequate stability of Cr within this substrate, and (ii) a small overlap of d- orbitals of Cr with p- orbitals of O and C for sarin and soman around 3.5 eV indicating the high affinity of Cr towards these CWAs. On the other hand, PDOS of Zn-Cr@graphene with sarin and soman, presented on **Fig. 5 (b)**, shows a significant shift of d- orbitals of Zn at lower energy level. Therefore, the absence of high energy d- orbitals of Zn causes a lack hybridization at Fermi level with p- orbitals of C (graphene) resulting in a decreased stability of Zn embedding onto a carbon substrate and a lack of overlapping with high energy states of CWAs atoms.

Moreover, the inclusion of Zn instead of Cr affects also the electronic properties of sarin and soman. Indeed, p- orbitals of O and C of CWAs, which are merged for Cr-Cr@graphene at ~ -6 eV, split into two distinctive peaks because of the proximity of sarin over soman to the metal when Zn is considered. This distinct electronic feature between Zn and Cr further illustrates the higher ability of Cr to ensure an efficient capture of the CWAs.
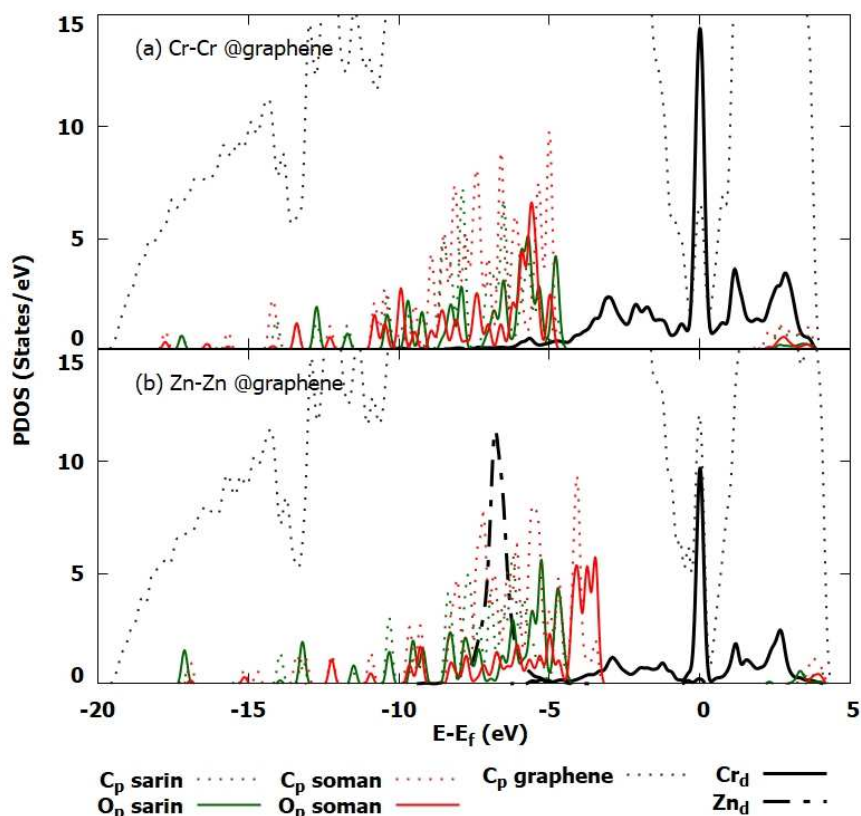
**Figure 5:** Comparison of PDOS for the sarin/soman on (a) Cr-Cr@graphene and (b) Cr-Zn@graphene substrate

## 6. Inclusion of water and effect on the competitive adsorption on a single site Cr@graphene

As a further step, we explored the competitive adsorption of CWAs with water on Cr and Zn adsorption site using first AIMD simulations followed by further DFT-geometry optimization. **Fig. 6 (a and b)** report the DFT-optimized, geometries of both sarin/soman/$H_2O$-Cr@graphene and sarin/soman/$H_2O$-Zn@graphene, respectively. Thus, adsorption energies calculated for sarin and soman on $H_2O$-Cr@graphene were found to be -26.04 kcal.mol$^{-1}$ and -25.21 kcal.mol$^{-1}$ respectively. This result is consistent with similar interacting distances for both sarin and soman with water as reported in **Fig. 6 (a)**. Indeed, the distances between the hydrogen atoms of water and the interacting oxygen atoms of sarin and soman are 1.62Å and 1.60Å respectively while the distance between water and Cr is equal to 1.98Å. This water molecule positioning enables an equivalent strength of interactions with sarin and soman. On the other hand, the adsorption energies for sarin and soman in the case of the $H_2O$-Zn@graphene analogue, i.e -17.65 kcal/mol$^{-1}$ and -23.08 kcal.mol$^{-1}$ respectively, demonstrate a more pronounced adsorption energy drop for sarin vs soman.
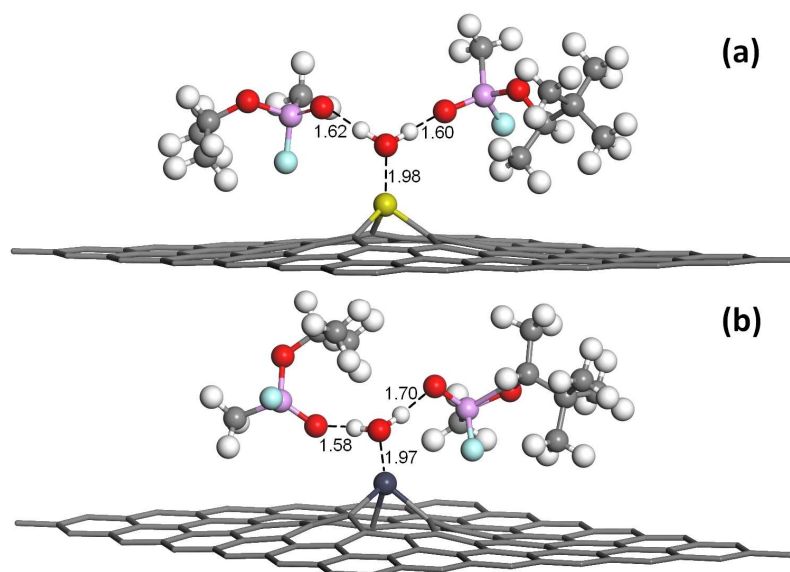
**Figure 6:** (a) Sarin/soman/H2O-Cr@graphene and (b) sarin/soman/H$_2$O-Zn@graphene DFT optimized structures. The reported distances are expressed in Å. C, O, F, P, H, Cr and Zn atoms are represented in grey, red, cyan, purple, white, yellow and dark blue respectively.

**Fig. 7 (a and b)** illustrates, from an electronically standpoint the adsorption energy variation of -8.39 kcal.mol$^{-1}$ reported for sarin interacting with H$_2$O-Cr@graphene vs H$_2$O-Zn@graphene. Similar electronic deformations were observed for water molecule adsorbed on both metal sites while the electronic behavior differs on the metals. Indeed, a symmetrical configuration takes place between sarin and soman on Cr@graphene where depletions of electronic charges are exclusively localized between the metal site and the water molecule. This leads to a preferential arrangement of the water molecule in such a way that its hydrogen atoms interact with both sarin and soman in a similar manner as reflected by the equivalent adsorption energy values reported for sarin and soman on H$_2$O-Cr@graphene. By contrast, the second configuration involving Zn presents a delocalization of the charge depletion region not only on the metal but also at the vicinity of sarin molecule. The absence of charges depletion on Zn metal allows strong interactions with the adsorbed water molecule and by extension to sarin and soman due to the lack of hybridization between high energy Zn d-states and the oxygen p-states present on all the considered components, i.e, water, sarin and soman. This observation is also responsible of the adsorption energy difference between sarin (-17.65 kcal/mol$^{-1}$) and soman (-23.08 kcal.mol$^{-1}$) on the same Zn metal site.
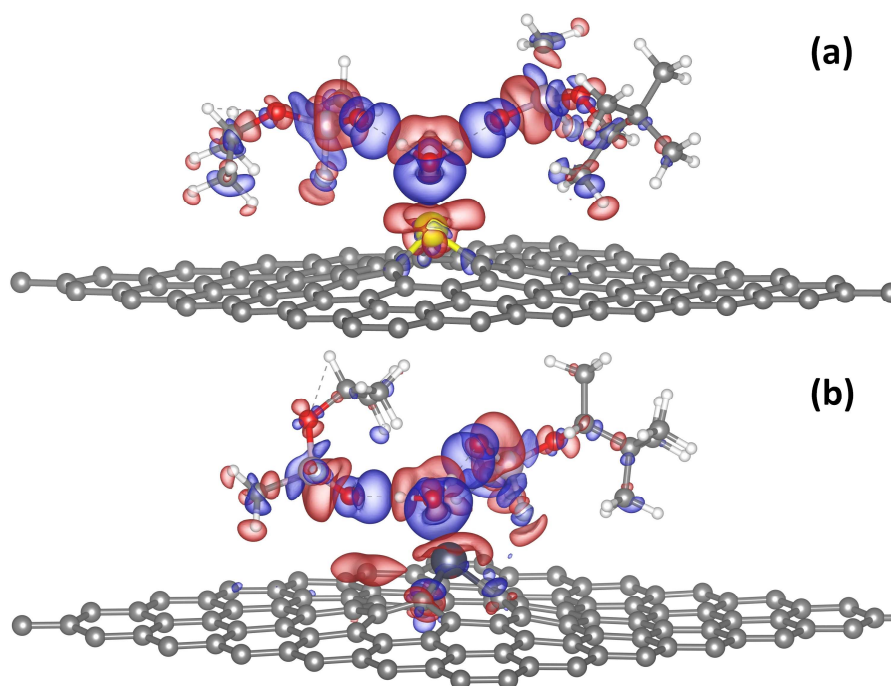
**Figure 7:** Charge differences of (a) sarin/soman/H$_2$O-Cr@graphene and (b) sarin/soman/H$_2$O-Zn@graphene complexes presented with isovalue of $\pm 1.0 \times 10^{-3} e.\text{Å}^{-3}$. Blue and red colors represent the charge accumulation and depletion regions respectively.

## 7. Conclusion

The simultaneous adsorption of sarin and soman on graphene activated carbons models embedding multiple metal sites (Vanadium, Chromium or Zinc) was computationally explored through subsequent AIMD and DFT simulations. This approach enabled us to accurately determine the preferential CWA adsorption sites and associated energetics on all these graphene models. We demonstrated that both CWAs adopt a single-adduct configuration on a metal site whatever the nature of the metal pairs considered, a scenario similar to that encountered for graphene containing only 1 metal site. This suggests that each metal site present in real activated carbons is effective for the CWA capture. We further revealed that water only moderately impact the adsorption energies between CWAs and both Cr and V metals while there is a substantial drop in the case of Zn metals. This trend was explained by PDOS analysis. This conclusion suggests that in contrast to Cr and V metals, the use of Zn metal does not enable to maintain an efficient capture of CWAs under humidity.

References

[1] S. Chauhan, R. D'cruz, S. Faruqi, K. Singh, S. Varma, M. Singh, V. Karthik, Chemical warfare agents, Environmental Toxicology and Pharmacology, 26 (2008) 113-122.
[2] A. Mangerich, C. Esser, Chemical warfare in the First World War: reflections 100 years later, Archives of Toxicology, 88 (2014) 1909-1911.
[3] T. Okumura, N. Takasu, S. Ishimatsu, S. Miyanoki, A. Mitsuhashi, K. Kumada, K. Tanaka, S. Hinohara, Report on 640 victims of the Tokyo subway sarin attack, Annals of emergency medicine, 28 (1996) 129-135.
[4] F. Barnaby, Iran-Iraq War: the use of chemical weapons against the Kurds, Ambio, 17 (1988) 407-408.
[5] J. Dingeman, R. Jupa, Chemical warfare in the Iran-Iraq conflict, Strategy & Tactics, 113 (1987) 51-52.
[6] K. Yokoyama, A. Yamada, N. Mimura, Clinical profiles of patients with sarin poisoning after the Tokyo subway attack, The American journal of medicine, 100 (1996) 586.
[7] G. Prasad, B. Singh, R. Vijayaraghavan, Respiratory protection against chemical and biological warfare agents, Defence Science Journal, 58 (2008) 686.
[8] B. Altshuler, J.F. Reynolds, Civilian anti-terrorist attack gas mask, in, Google Patents, 2004.
[9] C.-Y. Lu, M.-Y. Wey, Simultaneous removal of VOC and NO by activated carbon impregnated with transition metal catalysts in combustion flue gas, Fuel Processing Technology, 88 (2007) 557-567.
[10] L. Hu, X. Hu, X. Wu, C. Du, Y. Dai, J. Deng, Density functional calculation of transition metal adatom adsorption on graphene, Physica B: Condensed Matter, 405 (2010) 3337-3341.
[11] H. Wang, Q. Wang, Y. Cheng, K. Li, Y. Yao, Q. Zhang, C. Dong, P. Wang, U. Schwingenschlögl, W. Yang, Doping monolayer graphene with single atom substitutions, Nano letters, 12 (2011) 141-144.
[12] M. Rafique, Y. Shuai, H.-P. Tan, H. Muhammad, Theoretical perspective on structural, electronic and magnetic properties of 3d metal tetraoxide clusters embedded into single and di-vacancy graphene, Applied Surface Science, 408 (2017) 21-33.
[13] A.V. Markevich, M. Baldoni, J.H. Warner, A.I. Kirkland, E. Besley, Dynamic behavior of single Fe atoms embedded in graphene, The Journal of Physical Chemistry C, 120 (2016) 21998-22003.
[14] A. Junkaew, C. Rungnim, M. Kunaseth, R. Arróyave, V. Promarak, N. Kungwan, S. Namuangruk, Metal cluster-deposited graphene as an adsorptive material for m-xylene, New Journal of Chemistry, 39 (2015) 9650-9658.
[15] K.-J. Kim, C.-S. Kang, Y.-J. You, M.-C. Chung, M.-W. Woo, W.-J. Jeong, N.-C. Park, H.-G. Ahn, Adsorption–desorption characteristics of VOCs over impregnated activated carbons, Catalysis Today, 111 (2006) 223-228.
[16] S. Wang, H. Ang, M.O. Tade, Volatile organic compounds in indoor environment and photocatalytic oxidation: state of the art, Environment international, 33 (2007) 694-705.
[17] J. Dai, J. Yuan, P. Giannozzi, Gas adsorption on graphene doped with B, N, Al, and S: a theoretical study, Applied Physics Letters, 95 (2009) 232105.
[18] D. Kaplan, L. Shmueli, I. Nir, D. Waysbort, I. Columbus, Degradation of adsorbed sarin on activated carbons: a 31P-MAS-NMR study, CLEAN–Soil, Air, Water, 35 (2007) 172-177.
[19] G. Wood, P. Lodewyckx, Correlations for High Humidity Corrections of Rate Coefficients for Adsorption of Organic Vapors and Gases on Activated Carbons in Air-Purifying Respirator Cartridges, JOURNAL-INTERNATIONAL SOCIETY FOR RESPIRATORY PROTECTION, 19 (2002) 58-64.

[20] G.O. Wood, Affinity coefficients of the Polanyi/Dubinin adsorption isotherm equations: A review with compilations and correlations, Carbon, 39 (2001) 343-356.

[21] P. Lodewyckx, E. Vansant, The influence of humidity on the overall mass transfer coefficient of the Wheeler-Jonas equation, AIHAJ-American Industrial Hygiene Association, 61 (2000) 461-468.

[22] T. Hall, P. BREYSSE, M. Corn, L. Jonas, Effects of adsorbed water vapor on the adsorption rate constant and the kinetic adsorption capacity of the Wheeler kinetic model, American Industrial Hygiene Association Journal, 49 (1988) 461-465.

[23] A.J. Fletcher, Y. Uygur, K.M. Thomas, Role of surface functional groups in the adsorption kinetics of water vapor on microporous activated carbons, The Journal of Physical Chemistry C, 111 (2007) 8349-8359.

[24] J.-C. Liu, P. Monson, Monte Carlo simulation study of water adsorption in activated carbon, Industrial & engineering chemistry research, 45 (2006) 5649-5656.

[25] A.J. Fletcher, Y. Yüzak, K.M. Thomas, Adsorption and desorption kinetics for hydrophilic and hydrophobic vapors on activated carbon, Carbon, 44 (2006) 989-1004.

[26] J. Lach, J. Goclon, P. Rodziewicz, Structural flexibility of the sulfur mustard molecule at finite temperature from Car–Parrinello molecular dynamics simulations, Journal of hazardous materials, 306 (2016) 269-277.

[27] S. Li, K. Song, D. Zhao, J.R. Rugarabamu, R. Diao, Y. Gu, Molecular simulation of benzene adsorption on different activated carbon under different temperatures, Microporous and Mesoporous Materials, (2020) 110220.

[28] R.H. Gee, I.-F.W. Kuo, S.C. Chinn, E. Raber, First-principles molecular dynamics simulations of condensed-phase V-type nerve agent reaction pathways and energy barriers, Physical Chemistry Chemical Physics, 14 (2012) 3316-3322.

[29] M.D. Esrafili, P. Nematollahi, H. Abdollahpour, A comparative DFT study on the CO oxidation reaction over Al-and Ge-embedded graphene as efficient metal-free catalysts, Applied Surface Science, 378 (2016) 418-425.

[30] H.-K. Dong, Y.-P. Wang, L.B. Shi, First principles study of HCN adsorption on graphene doped with 5d transition metal, Surface Review and Letters, 23 (2016) 1550095.

[31] C. Tabtimsai, T. Somtua, T. Motongsri, B. Wanno, A DFT study of H 2 CO and HCN adsorptions on 3d, 4d, and 5d transition metal-doped graphene nanosheets, Structural Chemistry, 29 (2018) 147-157.

[32] C. Vieira Soares, G. Maurin, A.A. Leitão, Computational Exploration of the Catalytic Degradation of Sarin and Its Simulants by a Titanium Metal–Organic Framework, The Journal of Physical Chemistry C, 123 (2019) 19077-19086.

[33] M. Agrawal, D.F. Sava Gallis, J.A. Greathouse, D.S. Sholl, How useful are common simulants of chemical warfare agents at predicting adsorption behavior?, The Journal of Physical Chemistry C, 122 (2018) 26061-26069.

[34] J. Claudot, E. Soubeyrand-Lenoir, G. Maurin, Computational exploration of Sarin and simulants adsorption on a series of transition metal embedded graphene, Applied Surface Science, (2020) 148047.

[35] J. Claudot, E. Soubeyrand-Lenoir, G. Maurin, Competitive adsorption of water and chemical warfare agents on transition metal embedded graphene, Applied Surface Science, (2020) Submitted.

[36] K. Suresh Kumar Reddy, A. Al Shoaibi, C. Srinivasakannan, Elemental mercury adsorption on sulfur-impregnated porous carbon–A review, Environmental technology, 35 (2014) 18-26.

[37] D.T. Doughty, J.E. Groose, Chromium-free impregnated activated carbon for adsorption of toxic gases and/or vapors, in, Google Patents, 1991.

[38] T.D. Kühne, M. Iannuzzi, M. Del Ben, V.V. Rybkin, P. Seewald, F. Stein, T. Laino, R.Z. Khaliullin, O. Schütt, F. Schiffmann, CP2K: An electronic structure and molecular dynamics software package-Quickstep: Efficient and accurate electronic structure calculations, The Journal of Chemical Physics, 152 (2020) 194103.

[39] J. VandeVondele, M. Krack, F. Mohamed, M. Parrinello, T. Chassaing, J. Hutter, Quickstep: Fast and accurate density functional calculations using a mixed Gaussian and plane waves approach, Computer Physics Communications, 167 (2005) 103-128.

[40] J. VandeVondele, J. Hutter, Gaussian basis sets for accurate calculations on molecular systems in gas and condensed phases, The Journal of chemical physics, 127 (2007) 114105.

[41] J.P. Perdew, Y. Wang, Accurate and simple analytic representation of the electron-gas correlation energy, Physical Review B, 45 (1992) 13244.

[42] S. Grimme, Semiempirical GGA-type density functional constructed with a long-range dispersion correction, Journal of computational chemistry, 27 (2006) 1787-1799.

[43] P. Giannozzi, S. Baroni, N. Bonini, M. Calandra, R. Car, C. Cavazzoni, D. Ceresoli, G.L. Chiarotti, M. Cococcioni, I. Dabo, QUANTUM ESPRESSO: a modular and open-source software project for quantum simulations of materials, Journal of physics: Condensed matter, 21 (2009) 395502.

[44] D. Vanderbilt, Soft self-consistent pseudopotentials in a generalized eigenvalue formalism, Physical review B, 41 (1990) 7892.

Soman                    Sarin